PCCP

ROYAL SOCIETY OF CHEMISTRY

PAPER

View Article Online
View Journal | View Issue



Cite this: *Phys. Chem. Chem. Phys.*, 2021, **23**, 22313

# An efficient implementation of spin–orbit coupling within the framework of semiempirical orthogonalization-corrected methods for ultrafast intersystem crossing dynamics†

Jie Liu, *[a] Zhenggang Lan [b] and Jinlong Yang *[a]

Received 29th July 2021,
Accepted 12th September 2021

DOI: 10.1039/d1cp03477d

rsc.li/pccp

We implement spin–orbit coupling (SOC) within the framework of semiempirical orthogonalization-corrected methods (OMx). The excited-state wavefunction is generated from configuration interaction with single excitations (CIS). The SOC Hamiltonian in terms of the one-electron Breit–Pauli operator with effective nuclear charges is adopted in this work. Benchmark calculations show that SOCs evaluated using the OMx/CIS method agree very well with those obtained from time-dependent density functional theory. As a particularly attractive application, we incorporate SOCs between singlet and triplet states into Tully's fewest switches surface hopping algorithm to enable excited-state nonadiabatic dynamics simulations, treating internal conversion and intersystem crossing on an equal footing. This semiempirical dynamics simulation approach is applied to investigate ultrafast intersystem crossing processes in core-substituted naphthalenediimides.



## 1 Introduction

The ability to unravel nonadiabatic dynamics processes in photophysical and photochemical phenomena is crucial in many fields of research, including photovoltaics, photocatalysis, photosynthesis and so on.[1–8] Theoretical models to study these photoinduced ultrafast internal conversion (IC) and intersystem crossing (ISC) processes involve time evolution of many electronic states, which often requires nonadiabatic molecular dynamics (NAMD) simulation methods,[9–13] such as trajectory-based surface hopping[14] and multiple spawning[15] approaches. Here, excited-state electronic structure properties including potential energy surfaces, energy gradients, nonadiabatic couplings and spin–orbit couplings (SOCs) of a manifold of electronic states are usually generated "on-the-fly" from electronic structure methods.[16]

Rapid progress in advanced electronic structure algorithms has extensively extended the rage of applicability of NAMD methods. For example, high-level wavefunction methods, such as the complete active space self-consistent field (CASSCF),[17,18] multi-reference configuration interaction (MRCI)[19,20] and complete active-space second-order perturbation (CASPT2)[21] methods, have been applied to accurately describe the excited-state dynamics of small nucleobase molecules.[13] These high-level methods have also been generalized to larger systems, such as the 51-atom provitamin $D_3$ molecule, through a combination of advanced algorithms and GPU-acceleration.[22] In contrast, single-reference methods, such as coupled cluster (CC) methods,[23–26] algebraic-diagrammatic construction (ADC) methods,[27,28] and time-dependent density functional theory (TDDFT),[29,30] enable NAMD simulations of medium-size systems,[1,10] such as vitamin D photosynthesis[31] and benzene excimer formation.[32] However, the applicability of NAMD methods to large systems is still challenging using these *ab initio* methods due to the high computational costs.

A particularly appealing possibility is to generalize semiempirical methods to NAMD dynamics simulations for large systems. For example, floating occupation molecular orbital CI (FOMO-CI),[33] semiempirical orthogonalization-corrected methods (OMx) MRCI,[34–36] time-dependent density functional tight binding (TDDFTB)[37] and the collective electronic oscillator (CEO) method applied at the Austin model 1 (AM1) level of theory in combination with a configuration interaction singles (CIS) formalism[38] have been successfully applied to a large variety of photoinduced ultrafast processes in organic molecules. Recently, Liu and Thiel combined the OMx methods including orthogonalization models OM1, OM2, and OM3[39,40] with configuration interaction with single excitations (CIS),

[a] *Hefei National Laboratory for Physical Sciences at Microscale, University of Science and Technology of China, Hefei, Anhui 230026, China. E-mail: liujie86@ustc.edu.cn, jlyang@ustc.edu.cn*

[b] *Guangdong Provincial Key Laboratory of Chemical Pollution and Environmental Safety and MOE Key Laboratory of Environmental Theoretical Chemistry, SCNU Environmental Research Institute, School of Environment, South China Normal University, Guangzhou 510006, P. R. China*

† Electronic supplementary information (ESI) available. See DOI: 10.1039/d1cp03477d

which includes all single excitations,[41] and the spin–flip extended configuration interaction with single excitations (SF-XCIS) method, which treats the ground state and excited states in a fully balanced manner and properly describes conical intersections involving the ground state.[42] Due to the explicit inclusion of Pauli exchange, the OMx/CIS and OMx/SF-XCIS methods give a promising description of excited-state properties and dynamic processes. Furthermore, to apply these methods for simulating intersystem crossing dynamics requires the evaluation of SOCs between singlet and triplet states.

A rigorous calculation of SOCs would use relativistic quantum mechanics, namely the Dirac equation, and include many-body interactions. In practical calculations, approximate schemes including variational methods, such as the zeroth-order regular approximation (ZORA),[43–45] and perturbative methods, such as the Breit–Pauli approximation,[46–49] have been proposed to reduce the computational costs. Here, the SOC Hamiltonian using the Breit–Pauli operator can be directly evaluated from excited-state wavefunctions and this has been widely implemented in quantum chemistry packages.[50–54] The Breit–Pauli operator contains one- and two-electron terms originating from the interaction of the electron spin with the orbital angular momentum. In addition, a reduced screened-nuclear charge method has also been proposed as a reformulation of the Breit–Pauli operator in terms of a single-electron operator together with effective nuclear charges.[46–49]

In this work, we present efficient evaluation of spin–orbit coupling within the framework of OMx/CIS. The simplest method using the one-electron term of the Breit–Pauli operator has been adopted for the SOC calculations. A scaling parameter, the effective nuclear charge, approximately accounts for the missing two-electron spin–orbit term in the Breit–Pauli operator. The formula of the effective nuclear charges used for OMx/CIS without reoptimization was originally derived by fitting experimental results for fine structure splittings in Π states of diatomic hydrides for the multiconfiguration self-consistent field (MCSCF) method with the effective core potential (ECP) basis set.[46,47] By incorporating the SOCs into Tully's fewest switches algorithm for surface hopping (FSSH),[9,14,55–57] one of most widely used mixed quantum-classical dynamics methods, we generalize the OMx/CIS method for simulating both internal conversion and intersystem crossing dynamics in large systems.

This paper is organized as follows. Section 2 gives a brief description of the theoretical methodology, covering the OMx methods, excited-state properties and spin–orbit couplings computed within the semiempirical OMx/CIS framework, and then the generalized FSSH method. More details about the numerical implementation of SOCs within the framework of OMx/CIS are discussed in Section 3. In Section 4, we benchmark SOCs for a set of small molecules evaluated at the OMx/CIS level with respect to the TDDFT and TDDFTB methods. After that, we present nonadiabatic dynamics simulations of ultrafast intersystem crossing processes in core-substituted naphthalenediimides,[58–62] which accounts for the high fluorescence quantum yields. A summary is given in Section 5.

# 2 Theoretical methodology

Let's introduce the notation used throughout this work. Lowercase italics $i,j$ label occupied molecular orbitals; $a,b$ label virtual molecular orbitals; and $p,q,r,s$ label arbitrary molecular orbitals. Greek letters $\mu,\nu$ label atomic orbitals (AOs). Two-electron integrals are defined as

$$(pq\sigma|rs\sigma') = \iint \frac{\phi_{p\sigma}(\mathbf{r})\phi_{p\sigma}(\mathbf{r})\phi_{r\sigma'}(\mathbf{r}')\phi_{s\sigma'}(\mathbf{r}')}{|\mathbf{r}-\mathbf{r}'|}\mathrm{d}\mathbf{r}\mathrm{d}\mathbf{r}'. \quad (1)$$

$\phi_{p\sigma}$ is the $p$th molecular orbital and $\varepsilon_{p\sigma}$ is the corresponding molecular orbital energy. $\sigma$ is the spin index and $\alpha,\beta$ indicate different spins. $N$ is the number of basis functions. $N_A$ is the number of atoms. Vectors and matrices are written in bold type.

## 2.1 OMx methods

Assuming the zero-differential-overlap approximation, the OMx working equation is given as

$$\mathbf{FC} = \mathbf{CE}, \quad (2)$$

where $\mathbf{C}$ is the molecular orbital (MO) coefficient and $\mathbf{E}$ is the diagonal matrix of the corresponding MO energies. The Fock matrix is given in the basis of molecular orbitals as

$$F_{pq\sigma} = h_{pq\sigma} + \sum_{i\sigma'}[(pq\sigma|ii\sigma') - (pi\sigma|iq\sigma)\delta_{\sigma\sigma'}], \quad (3)$$

where $\mathbf{h}$ is the one-electron core Hamiltonian including one-electron energies, semiempirical core–electron attractions, valence orthogonalization corrections, penetration integrals and effective core potentials (see ref. 39 for a detailed expression). The explicit inclusion of orthogonalization terms in the OMx methods offers significant improvements in the description of asymmetric splitting of bonding and antibonding orbitals, which is crucial for performing excited-state dynamics simulations.[35,36,39,40]

In order to achieve a low-scaling quantum-chemical method, the OMx methods expand the molecular orbitals $\phi$ in a set of orthogonal minimal valence atomic orbitals $\chi^{\perp}$,

$$\phi_{p\sigma} = \sum_{\mu} C_{\mu p\sigma}\chi^{\perp}_{\mu}. \quad (4)$$

Standard four-center two-electron integrals scale as $O(N^4)$. In the OMx method, only the two-center two-electron integrals $(\mu^A\nu^A|\lambda^B\kappa^B)$ involved in the Fock matrix are evaluated by the analytical integrals over the contracted Gaussian valence orbitals with a uniform Klopman–Ohno scaling.[39] This leads to a much lower computational scaling as $\mathcal{O}(N^2)$. In OM2 and OM3, there exist three-center orthogonalization corrections that in principle scale as $\mathcal{O}(N^3)$ for matrix multiplications. The feature of the low-scaling computational cost enables the application of the OMx methods to study large systems containing hundreds of atoms.

 

### 2.2 CIS method

The singlet and triplet excitation configurations can be expressed as

$$|\mathrm{S}_i^a\rangle = \frac{\sqrt{2}}{2}(\psi_{i\alpha}^{a\alpha} + \psi_{i\beta}^{a\beta}) \quad |\mathrm{T}_i^a\rangle_{1,1} = \psi_{i\beta}^{a\alpha}$$
$$|\mathrm{T}_i^a\rangle_{1,-1} = \psi_{i\alpha}^{a\beta} \quad |\mathrm{T}_i^a\rangle_{1,0} = \frac{\sqrt{2}}{2}(\psi_{i\alpha}^{a\alpha} - \psi_{i\beta}^{a\beta}) \tag{5}$$

where the subscript $(l,m)$ indicates the angular and magnetic quantum numbers, respectively, and "S" and "T" indicate singlet and triplet configurations, respectively. Here, we assume a single excitation promoting an electron from an occupied orbital $i$ to an unoccupied orbital $a$.

The CIS wavefunction is defined as

$$\Psi_{\mathrm{CIS}} = \sum_{ai} X_{ai}\psi_i^a, \tag{6}$$

with $\psi_i^a$ defined in eqn (5). The excitation energy $\omega_I$ and the amplitude $\mathbf{X_I}$ can be obtained from the CIS eigenvalue equation,

$$\mathbf{AX_I} = \omega_I\mathbf{X_I}. \tag{7}$$

The matrix elements of $\mathbf{A}$ are defined in the basis of molecular orbitals as follows

$$\langle\psi_{i\sigma}^{a\sigma}|A|\psi_{j\sigma'}^{b\sigma'}\rangle = \delta_{ab}\delta_{ij}\delta_{\sigma\sigma'}(\varepsilon_a - \varepsilon_i) + (ai\sigma|bj\sigma') - (ab\sigma|ij\sigma)\delta_{\sigma\sigma'}$$
$$\langle\psi_{i\sigma}^{a\sigma'}|A|\psi_{j\sigma}^{b\sigma'}\rangle = \delta_{ab}\delta_{ij}(\varepsilon_a - \varepsilon_i) - (ab|ij) \tag{8}$$

In this work, we assume closed-shell molecular orbitals used throughout this work. For simplicity, we drop the spin labels and rewrite eqn (9) as

$$A_{ai,bj}^{\mathrm{S}} = \delta_{ab}\delta_{ij}(\varepsilon_a - \varepsilon_i) + 2(ai|bj) - (ab|ij)$$
$$A_{ai,bj}^{\mathrm{T}} = \delta_{ab}\delta_{ij}(\varepsilon_a - \varepsilon_i) - (ab|ij) \tag{9}$$

The summation over the spin index is absorbed in the coefficients. The Coulomb part $(ai|bj)$ vanishes for triplet excitations since the single excitation, $i \to a$, has opposite spin for $|\mathrm{T}_i^a\rangle_{1,1}$ and $|\mathrm{T}_i^a\rangle_{1,-1}$ or the integral cancels itself out for $|\mathrm{T}_i^a\rangle_{1,0}$. The transition vectors $\mathbf{X}$ satisfy

$$\mathbf{X}_I^\dagger\mathbf{X_J} = \delta_{IJ}. \tag{10}$$

The $I$th excitation energy is given by

$$\omega_I = \langle\mathbf{X_I}|\mathbf{A}|\mathbf{X_I}\rangle. \tag{11}$$

To extract a few excited states within a specified energy window for large systems, the Davidson iterative algorithm[63] is one of the most widely used methods to diagonalize the eigenvalue equation. It reduces the scaling of the OMx/CIS method from $\mathcal{O}(n^6)$ to $\mathcal{O}(n^3)$ by projecting the eigenvalue equation onto an appropriate subspace instead of diagonalizing the whole matrix. Considering that only two-center two-electron integrals are required in eqn (9), the OMx/CIS method is computationally efficient for excited-state dynamics simulations of molecular systems with dozens of atoms.

### 2.3 Spin–orbital coupling

The Dirac equation, describing the wavefunction with four components, is in principle a rigorous scheme to account for spin–orbit coupling. However, due to its high computational cost, approximate strategies are frequently used to evaluate spin–orbital coupling in practical calculations. In this work, we have implemented the simplest spin–orbit Hamiltonian *via* the one-electron Breit–Pauli operator and embodied effective nuclear charges

$$\hat{H}_{\mathrm{SOC}}^{\mathrm{eff}} = \sum_m^{N_e}\hat{\mathbf{l}}_m\cdot\hat{\mathbf{s}} \tag{12}$$

where $\hat{\mathbf{l}}_m$ is the orbital angular momentum operator for electron $m$,

$$\hat{\mathbf{l}}_m = \frac{\alpha_0^2}{2}\sum_{\mathrm{A}}^{N_{\mathrm{A}}}\frac{Z_{\mathrm{A}}^{\mathrm{eff}}}{r_{m\mathrm{A}}^3}\hat{\mathbf{r}}_{m\mathrm{A}}\times\hat{\mathbf{p}}_m, \tag{13}$$

and $\hat{\mathbf{s}}$ is the spin angular momentum operator,

$$\hat{s}_x = \begin{bmatrix}0 & 1\\ 1 & 0\end{bmatrix}, \quad \hat{s}_y = \begin{bmatrix}0 & -i\\ i & 0\end{bmatrix}, \quad \hat{s}_z = \begin{bmatrix}1 & 0\\ 0 & -1\end{bmatrix}. \tag{14}$$

$Z_{\mathrm{A}}^{\mathrm{eff}}$ is the effective charge on nucleus A and fine-structure constant $\alpha_0 = e/m_e c$.

Given singlet and triplet wavefunctions

$$|\Psi_{\mathrm{S}}\rangle = \sum_{ai}X_{ai}^{\mathrm{S}}|\mathrm{S}_i^a\rangle \quad |\Psi_{\mathrm{T}}\rangle_{1,-1} = \sum_{ai}X_{ai}^{\mathrm{T}}|\mathrm{T}_i^a\rangle_{1,-1}$$
$$|\Psi_{\mathrm{T}}\rangle_{1,0} = \sum_{ai}X_{ai}^{\mathrm{T}}|\mathrm{T}_i^a\rangle_{1,0} \quad |\Psi_{\mathrm{T}}\rangle_{1,1} = \sum_{ai}X_{ai}^{\mathrm{T}}|\mathrm{T}_i^a\rangle_{1,1} \tag{15}$$

the spin–orbit couplings between a singlet ground state and a triplet excited state are

$$\langle\Psi_0|\hat{H}_{\mathrm{soc}}^{\mathrm{eff}}|\Psi_T\rangle_{1,1} = \frac{\sqrt{2}}{2}\sum_{ia}t_i^a(l_{xia} + il_{yia})$$
$$\langle\Psi_0|\hat{H}_{\mathrm{soc}}^{\mathrm{eff}}|\Psi_T\rangle_{1,0} = \sum_{ia}t_i^a l_{zia} \tag{16}$$
$$\langle\Psi_0|\hat{H}_{\mathrm{soc}}^{\mathrm{eff}}|\Psi_T\rangle_{1,-1} = \frac{\sqrt{2}}{2}\sum_{ia}t_i^a(l_{xia} - il_{yia})$$

and the spin–orbit couplings between singlet and triplet excited states are

$$\langle\Psi_{\mathrm{S}}|\hat{H}_{\mathrm{SOC}}^{\mathrm{eff}}|\Psi_{\mathrm{T}}\rangle_{1,1} = \frac{\sqrt{2}}{2}\sum_{iab}s_i^b t_i^a(l_{xba} + il_{yba}) - \frac{\sqrt{2}}{2}\sum_{ija}s_j^b t_i^a(l_{xij} + il_{yij})$$
$$\langle\Psi_{\mathrm{S}}|\hat{H}_{\mathrm{SOC}}^{\mathrm{eff}}|\Psi_{\mathrm{T}}\rangle_{1,0} = \sum_{iab}s_i^b t_i^a l_{zab} - \sum_{ija}s_i^a t_j^a l_{zji} \tag{17}$$
$$\langle\Psi_{\mathrm{S}}|\hat{H}_{\mathrm{SOC}}^{\mathrm{eff}}|\Psi_{\mathrm{T}}\rangle_{1,-1} = \frac{\sqrt{2}}{2}\sum_{iab}s_i^b t_i^a(l_{xba} - il_{yba}) - \frac{\sqrt{2}}{2}\sum_{ija}s_j^b t_i^a(l_{xij} - il_{yij})$$

Here, we define

$$s_i^a = \frac{\sqrt{2}}{2} X_{ai}^{\mathrm{S}}, \quad t_i^a = \frac{\sqrt{2}}{2} X_{ai}^{\mathrm{T}} \tag{18}$$

which are the CIS amplitudes defined in most quantum chemistry packages.

The total spin–orbit coupling between one pair of singlet and triplet states is given as

$$H_{\mathrm{ST}}^{\mathrm{SOC}} = \left( \sum_{m=1,0,-1} |\langle \Psi_{\mathrm{S}} | \hat{H}_{\mathrm{SOC}}^{\mathrm{eff}} | \Psi_{\mathrm{T}} \rangle_{1,m}|^2 \right)^{1/2} \tag{19}$$

### 2.4 Generalized trajectory surface-hopping method

The trajectory surface-hopping (TSH) method is a popular tool to study ultrafast ISC processes. For example, the TSH method has been combined with Landau–Zener,[64] Zhu–Nakamura theory,[65] or ''on-the-fly'' SOCs for ISC dynamics simulations.[11–13] In the latter case, the Tully's fewest switches TSH method has been applied to study ISC processes in both spin-adiabatic and spin-diabatic representations.[13,66–71] When the SOC is relatively small and the states closely approach each other, it is promising to perform the TSH dynamics in the spin-diabatic representation.[68,72–74]

Considering the spin–orbit coupling as a perturbation interaction in the Hamiltonian[68–70]

$$\hat{H}[\mathbf{r},\mathbf{R}(t)] = \hat{H}_0[\mathbf{r},\mathbf{R}(t)] + \hat{H}^{\mathrm{SOC}}[\mathbf{r},\mathbf{R}(t)] \tag{20}$$

where $\hat{H}_0$ is the spin-free part of the Hamiltonian, the time-dependent wavefunction can be expressed in terms of eigenstates of $\hat{H}_0$

$$\Psi[\mathbf{r},\mathbf{R}(t)] = \sum_I c_I(t) \Psi_0^I[\mathbf{r},\mathbf{R}(t)], \tag{21}$$

with

$$\hat{H}_0 \Psi_0^I[\mathbf{r},\mathbf{R}(t)] = E_I[\mathbf{R}(t)] \Psi_0^I[\mathbf{r},\mathbf{R}(t)] \tag{22}$$

and $c_I$ being the coefficient of the $I$-th electronic state. Inserting eqn (21) into the time-dependent Schrödinger equation, the generalized FSSH working equation is given as

$$\begin{aligned} \dot{c}_J(t) \;=\; & -i\hbar^{-1} \left[ c_J(t) E_J[\mathbf{R}(t)] + \sum_I c_I(t) H_{JI}^{\mathrm{SOC}}[\mathbf{R}(t)] \right] \\ & - \sum_I c_I(t) D_{JI}(t) \end{aligned} \tag{23}$$

The nonadiabatic coupling is defined as

$$D_{JI}(t) = \left\langle \Psi_0^I \middle| \frac{\partial}{\partial t} \Psi_0^J \right\rangle. \tag{24}$$

The detailed expression of $D_{IJ}$ within the framework of OMx/CIS is formulated in ref. 41. The hopping probability from state $I$ to state $J$ is written as

$$P_J(t)\mathrm{d}t = 2 \frac{\mathrm{Re}(c_I^* c_J D_{IJ}) - \mathrm{Im}(\hbar^{-1} c_I^* c_J H_{IJ}^{\mathrm{SOC}})}{c_I^* c_I} \mathrm{d}t. \tag{25}$$

In this work, a simple spin-diabatic representation with each state considered as a single electronic state has been used to account for the spin–orbit coupling.[68,72–74] The effective SOCs are defined as

$$\left( \frac{1}{3} \sum_{m=1,0,-1} |\langle \Psi_{\mathrm{S}} | \hat{H}_{\mathrm{SOC}}^{\mathrm{eff}} | \Psi_{\mathrm{T}} \rangle_{1,m}|^2 \right)^{1/2}, \tag{26}$$

namely, we approximate it by averaging over the interactions between the singlet and the three triplet sublevels (this is analogous to the definition of the effective SOC used in ref. 68). In this way, the effective SOC values for singlet–triplet transitions are the same in either direction. This approach suffers from an incorrect description of intersystem crossing in certain cases as the sign change of SOCs occurs as the two states come close in energy. As such, Granucci and coworkers have recommended, when possible, the spin-adiabatic representation to be used, which needs the diagonalization of the full electronic Hamiltonian.[67,69,71] However, in complex molecular systems, this situation is expected to rarely happen and therefore we are able to use the spin-diabatic approach to obtain a qualitative result as long as one is aware of its limitations.

The surface hopping method implemented in the spin-adiabatic representation has been successfully used in studying ultrafast intersystem crossing for nucleobases and DNA molecules,[13,75,76] and transition metal complexes.[77] Due to the lack of a calculation of energy gradients including SOCs in most quantum chemistry software packages, some approximations should be introduced in the spin-adiabatic representation as discussed in ref. 13. In this work, we demonstrate a proof-of-principle application of the OMx/CIS method to ISC dynamics. Further work is needed in the future to explore better representations of the effective SOC Hamiltonian or to interface the MNDO program to advanced dynamics simulation software, such as SHARC,[13] and NEXTON-X,[50] to enable more choice of the spin basis representation.

## 3 Implementation

An efficient implementation of excited-state calculations including vertical excitation energies, analytic excite-state gradients and nonadiabatic couplings within the framework of OMx/CIS has been realized in the semiempirical MNDO electronic structure package.[78] In this work, we focus on the implementation of the spin–orbital coupling at the OMx/CIS level and combining it with the generalized trajectory surface-hopping method. The CIS wavefunction can be explicitly extracted from the OMx/CIS calculation. One main task is to implement orbital angular momentum integrals over contracted Gaussian atomic orbitals (STO-3G for hydrogen and ECP-3G for carbon, nitrogen, oxygen, and fluorine). Since these integrals are one-electron integrals and only a minimal atomic basis is used in the OMx method, we adopt the Obara and Saika scheme for evaluating the matrix elements of orbital angular momentum operators in eqn (13).

 

As stated above, we have implemented a reduced screened-nuclear charge method in this work. The effective nuclear charges ($Z_{\text{eff}}$),[46,79]

$$\begin{aligned} Z_{\text{eff}} &= f_m Z \\ f_1 &= 0.45 + 0.05 \times N_{\text{val}} \quad \text{for Li}-\text{F} \\ f_2 &= 12 \quad \text{for Na}-\text{Cl} \\ f_3 &= 41 \quad \text{for K, Ca, Ge}-\text{Br} \end{aligned} \tag{27}$$

which are empirical parameters in the single-electron spin–orbit Hamiltonian of eqn (12), are determined for main group elements by using experimental results for the fine structure splittings in Π states of diatomic hydrides. Here, $Z$ is the true nuclear charge and $N_{\text{val}}$ is the number of valence electrons. Note that eqn (27) was initially optimized for the MCSCF/SBK method with the ECP basis set designed by Stevens, Basch and Krauss.[80] However, as shown in the following benchmark, incorporating this $Z_{\text{eff}}$ expression in the OMx/CIS methods, the accuracy of SOCs is also quite promising.

For the evaluation of SOCs with all-electron basis sets, a different expression of $Z_{\text{eff}}$ should be used[81]

$$\begin{aligned} f_1 &= 0.2517 + 0.0626 \times N_{\text{val}} \quad \text{for B}-\text{F} \\ f_2 &= 0.7213 + 0.0144 \times N_{\text{val}} \quad \text{for Al}-\text{Cl} \\ f_3 &= 0.8791 + 0.003942 \times N_{\text{val}} \quad \text{for Ga}-\text{Br} \end{aligned} \tag{28}$$

which is applied in the TDDFT calculations for a more reasonable comparison with OMx/CIS.

Integral derivatives with respect to nuclear coordinates that appear in the one-electron and two-electron terms of excited-state gradients and nonadiabatic coupling are evaluated with the central finite difference (CFD) method. The evaluation of spin–orbital coupling does not need integral derivatives, while the orbital angular momentum operator results in one-electron integrals over higher angular momentum Gaussian functions. The overall computational cost of SOCs is still relatively low. In the integral calculations for OMx, one adjustable parameter $\zeta$ that scales the exponents of all Gaussian primitives has been introduced for fine-tuning of the computational accuracy. These scale factors are optimized to be greater than 1 in the OMx methods. For the SOC evaluations, all scale factors $\zeta$ are set to be 1 since the nuclear charges have been scaled to fit the experimental results.[46]

# 4 Results

All spin–orbit coupling calculations are performed using the one-electron Breit–Pauli operator with an effective nuclear charge approximation implemented in modified MNDO[78] and Q-Chem[52] electronic structure packages. The molecular structures for the SOC benchmark calculations are obtained from the literature[36,82] and drawn with VESTA.[83] For comparison purposes, different effective nuclear charge expressions of eqn (27) and (28) are used in MNDO and Q-Chem, respectively. Excited-state wavefunctions are generated using OMx/CIS from MNDO or linear-response TDDFT (LR-TDDFT) from Q-Chem.

## 4.1 Spin–orbit coupling

The molecular structures for the benchmark calculations are shown in Fig. 1. Correlation-consistent basis set cc-pVTZ is applied to all LR-TDDFT calculations. Due to the lack of parameterization of sulfur atoms in OM1 and OM3, we only present OM2 results for thymine derivatives (g–j) and the psoralen series (k–m). As discussed in ref. 82, the SOCs evaluated with different density functionals showed an obvious discrepancy. For example, the SOCs evaluated with PBE and ωB97XD differ by about 30 $\text{cm}^{-1}$ for $S_0/T_1$ of 2-thiothymine while the difference among various hybrid functionals is much smaller. Therefore, in this work one typical hybrid functional (B3LYP)[84] and one popular long-range corrected functional (ωB97XD)[85] are chosen for comparison. In addition, SOCs evaluated with TDDFTB (data from ref. 82) for thymine derivatives and psoralen derivatives are presented for comparison.

Table 1 lists the SOCs for formaldehyde, acetone and acrolein, in which there exist lowest-lying n → π* singlet and triplet excited states followed by the p → π* excited state. In comparison with LR-TDDFT, the OMx/CIS methods give a qualitatively correct description of strong SOCs, namely $^1\text{gs}/^3\text{n}\pi^*$ and $^1\text{n}\pi^*/^3\pi\pi^*$, for the three molecular systems. These results are also consistent with the El-Sayed rule that states that a radiationless transition from the lowest singlet states to the triplet manifold is relative large if this transition involves a change of molecular orbital type. In detail, the SOCs of $^1\text{n}\pi^*/^3\pi\pi^*$ evaluated with OMx/CIS agree quite well with those evaluated with LR-TDDFT in formaldehyde and acetone, while in acrolein the SOCs of $^1\text{n}\pi^*/^3\pi\pi^*$ evaluated with OMx/CIS and LR-TDDFT differ by about 10 $\text{cm}^{-1}$. For the SOCs of $^1\text{gs}/^3\text{n}\pi^*$ in the three systems, the OMx/CIS methods obviously underestimate them by about 10 $\text{cm}^{-1}$ compared with LR-TDDFT.

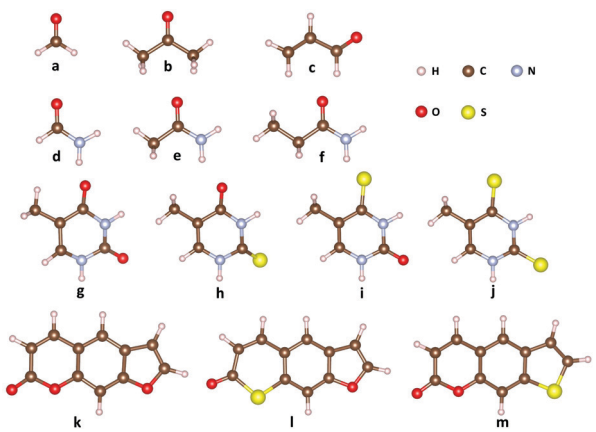


Fig. 1 Molecular structures for the spin–orbit coupling benchmark calculations: (a) formaldehyde, (b) acetone, (c) acrolein, (d) formamide, (e) acetamide, (f) propanamide, (g) thymine, (h) 2-thiothymine, (i) 4-thiothymine, (j) 2,4-thiothymine, (k) 7*H*-furo[3,2-*g*][1]benzopyran-7-one (psoralenOO), (l) 7*H*-thiopyrano[3,2-*f*][1]benzofuran-7-one (psoralenOS), and (m) 2*H*-thieno[3,2-*g*][1]benzopyran-2-one (psoralenSO).

Table 1 SOCs (in $cm^{-1}$) for formaldehyde, acetone and acrolein computed with OMx/CIS and LR-TDDFT using B3LYP and ωB97XD

| | $^1gs/^3\pi\pi^*$ | $^1gs/^3n\pi^*$ | $^1n\pi^*/^3\pi\pi^*$ | $^1n\pi^*/^3n\pi^*$ |
|---|---|---|---|---|
| Formaldehyde | | | | |
| OM1 | 0 | 49 | 45 | 0 |
| OM2 | 0 | 49 | 44 | 0 |
| OM3 | 0 | 50 | 40 | 0 |
| B3LYP | 0 | 61 | 46 | 0 |
| ωB97XD | 0 | 60 | 45 | 0 |
| Acetone | | | | |
| OM1 | 0 | 46 | 45 | 0 |
| OM2 | 1 | 43 | 43 | 0 |
| OM3 | 1 | 44 | 42 | 0 |
| B3LYP | 0 | 57 | 44 | 0 |
| ωB97XD | 0 | 57 | 44 | 0 |
| Acrolein | | | | |
| OM1 | 1 | 45 | 16 | 0 |
| OM2 | 1 | 43 | 15 | 0 |
| OM3 | 1 | 42 | 12 | 0 |
| B3LYP | 0 | 54 | 25 | 0 |
| ωB97XD | 0 | 54 | 23 | 0 |

However, the weak SOCs evaluated with the OMx/CIS methods are almost the same as those evaluated with LR-TDDFT.

Analogous to formaldehyde, acetone and acrolein, another set of molecules including formamide, acetamide and propanamide also have a carbonyl group that leads to lowest-lying n → p* states. However, this state has a much high excitation energy due to the amino-group substituent. Table 2 lists the SOCs between singlet states and low-lying triplet states in formamide, acetamide and propanamide. Compared with formaldehyde, acetone and acrolein, the SOCs of $^1gs/^3n\pi^*$ and $^1n\pi^*/^3\pi\pi^*$ in formamide, acetamide and propanamide only slightly decrease. The SOCs evaluated with OM1/CIS, OM2/CIS and OM3/CIS with respect to the LR-TDDFT results are very close each other except that the OM3/CIS method gives a relatively large value for the weak SOC of $^1gs/^3\pi\pi^*$. In addition, the difference in the SOCs between OM1/CIS and OM3/CIS is obvious, especially for $^1n\pi^*/^3\pi\pi^*$.

Table 2 SOCs (in $cm^{-1}$) for formamide, acetamide and propanamide computed with OMx/CIS and LR-TDDFT using B3LYP and ωB97XD

| | $^1gs/^3\pi\pi^*$ | $^1gs/^3n\pi^*$ | $^1n\pi^*/^3\pi\pi^*$ | $^1n\pi^*/^3n\pi^*$ |
|---|---|---|---|---|
| Formamide | | | | |
| OM1 | 2 | 46 | 42 | 1 |
| OM2 | 3 | 45 | 39 | 1 |
| OM3 | 11 | 44 | 35 | 1 |
| B3LYP | 1 | 54 | 39 | 0 |
| ωB97XD | 1 | 53 | 39 | 0 |
| Acetamid | | | | |
| OM1 | 2 | 44 | 42 | 0 |
| OM2 | 2 | 42 | 39 | 0 |
| OM3 | 3 | 41 | 37 | 1 |
| B3LYP | 0 | 52 | 40 | 0 |
| ωB97XD | 0 | 52 | 34 | 0 |
| Propanamide | | | | |
| OM1 | 2 | 44 | 42 | 0 |
| OM2 | 3 | 41 | 39 | 0 |
| OM3 | 4 | 41 | 36 | 0 |
| B3LYP | 0 | 51 | 39 | 0 |
| ωB97XD | 0 | 51 | 39 | 0 |

Table 3 SOCs (in $cm^{-1}$) for thymine, 2-thiothymine, 4-thiothymine, and 2,4-thiothymine computed with OM2/CIS and LR-TDDFT using B3LYP and ωB97XD

| | $^1gs/^3\pi\pi^*$ | $^1gs/^3n\pi^*$ | $^1n\pi^*/^3\pi\pi^*$ | $^1n\pi^*/^3n\pi^*$ |
|---|---|---|---|---|
| Thymine | | | | |
| OM2 | 4 | 35 | 10 | 6 |
| TD-B3LYP | 5 | 38 | 18 | 3 |
| TD-ωB97XD | 5 | 40 | 17 | 1 |
| TDDFTB | 5 | 39 | 32 | 4 |
| 2-Thiothymine | | | | |
| OM2 | 102 | 152 | 150 | 44 |
| TD-B3LYP | 108 | 151 | 132 | 68 |
| TD-ωB97XD | 108 | 153 | 141 | 50 |
| TDDFTB | 180 | 129 | 85 | 197 |
| 4-Thiothymine | | | | |
| OM2 | 2 | 110 | 120 | 1 |
| TD-B3LYP | 2 | 130 | 137 | 2 |
| TD-ωB97XD | 1 | 131 | 133 | 1 |
| TDDFTB | 1 | 175 | 206 | 0 |
| 2,4-Thiothymine | | | | |
| OM2 | 5 | 111 | 123 | 1 |
| TD-B3LYP | 3 | 135 | 135 | 3 |
| TD-ωB97XD | 2 | 134 | 136 | 1 |
| TDDFTB | 1 | 119 | 119 | 0 |

Table 3 lists SOCs for thymine and its thio-derivatives, including 2-thiothymine, 4-thiothymine and 2,4-thiothymine, evaluated with OM2/CIS and LR-TDDFT. As the heavy sulfur atom is introduced, the SOCs in the three sulfur-substituted thymine derivatives are significantly larger than those in thymine. On the other hand, due to the distorted out-of-plane structure, there exists strong *n*/mixing in the HOMO and HOMO-1 orbitals of 2-thiothymine. As such, 2-thiothymine has strong SOCs for $^1gs/^3\pi\pi^*$ and $^1n\pi^*/^3\pi\pi^*$, which break the El-Sayed rule. This is different from the other three thymine derivatives with planar structures. For all cases shown in Table 3, the SOCs predicted by the OM2/CIS method are quite close to the LR-TDDFT results with a largest error of 24 $cm^{-1}$. In contrast, as discussed in ref. 82, the difference between LR-TDDFT/ωB97XD and TDDFTB is as large as ~140 $cm^{-1}$ for $S_1/T_2$ in 2-thiothymine. For weak SOCs, OM2/CIS gives quite reasonable results.

Psoralen and its thio-derivatives have been well studied in previous work.[82,86,87] Table 4 shows four typical SOCs evaluated with OM2/CIS and LR-TDDFT. As the size of the systems increases, the ordering of excited states becomes more complicated when different methods are used. In order to perform a reliable comparison, SOCs between different electronic states are identified by the dominant excitation configuration for different methods. As usual, the calculated SOCs from different theoretical methods differ by less than 1 $cm^{-1}$ in the weak SOC case. The strong SOCs are systematically underestimated by OM2/CIS, especially for psoralenOS. In the case of $S_1/T_4$ for psoralenOS, the SOCs between OM2/CIS and TD-B3LYP differ by 27 $cm^{-1}$ while TDDFTB significantly overestimates it by 27 $cm^{-1}$. In addition, TDDFTB remarkably underestimates the SOC of $S_0/T_5$ for psoralenOO while OM2/CIS shows a much smaller deviation with respect to LR-TDDFT.

Table 4 SOCs (in $cm^{-1}$) for psoralenOO, psoralenOS and psoralenSO computed with OMx/CIS and LR-TDDFT using B3LYP and ωB97XD

| | OM2 | B3LYP | ωB97XD | TDDFTB |
|---|---|---|---|---|
| PsoralenOO | | | | |
| $S_0/T_1$ | 0 | 1 | 1 | 0 ($S_0/T_3$) |
| $S_0/T_5$ | 33 | 44 ($S_0/T_4$) | 48 | 32 ($S_0/T_2$) |
| $S_1/T_1$ | 0 | 1 | 1 | 0 ($S_2/T_3$) |
| $S_1/T_5$ | 6 | 9 ($S_1/T_4$) | 10 | 12 ($S_2/T_2$) |
| PsoralenOS | | | | |
| $S_0/T_1$ | 1 | 0 | 0 | 0 ($S_0/T_3$) |
| $S_0/T_4$ | 51 ($S_0/T_3$) | 72 | 77 | 75 ($S_0/T_2$) |
| $S_1/T_1$ | 0 | 0 | 0 | 0 ($S_2/T_3$) |
| $S_1/T_4$ | 8 ($S_1/T_3$) | 35 | 32 | 62 ($S_2/T_2$) |
| PsoralenSO | | | | |
| $S_0/T_1$ | 1 | 0 | 1 | 0 ($S_0/T_3$) |
| $S_0/T_5$ | 33 | 43 ($S_0/T_4$) | 48 | 30 ($S_0/T_2$) |
| $S_1/T_1$ | 1 | 1 | 1 | 1 ($S_2/T_3$) |
| $S_1/T_5$ | 5 | 4 ($S_1/T_4$) | 6 | 5 ($S_2/T_2$) |

Overall, the SOCs evaluated with the semiempirical OMx/CIS methods show good agreement with those obtained from LR-TDDFT with B3LYP and ωB97XD and the cc-pVTZ basis set. However, due to the minimal valence basis used in the OMx methods and the error from the CIS method, OMx/CIS systematically underestimates the SOCs for the benchmark molecular set. Considering that a scale factor $\zeta$ of 1 has been used without optimization for calculations of SOCs, it is possible to improve the accuracy of SOCs evaluated at the OMx/CIS level *via* optimizing each scale factor for different atoms.

### 4.2 Excited-state dynamics

In the past few years, core-substituted naphthalenediimides (c-NDIs) have aroused lots of interest as building blocks for application in photovoltaics, artificial photosysthesis and so on.[88–95] Typically, c-NDIs exhibit larger quantum fluorescence yields than the non-core-substituted naphthalenediimides. This mainly results from the change of excitation configurations in the lowest excited state induced by the core substituents. In this work, we apply the generalized surface hopping approach based on the OMx/CIS method to study ultrafast intersystem-crossing dynamics in a red naphthalenediimide (rNDI) dye.

In this work, all calculations are performed for an analogue of rNDI (m-rNDI), in which a hydrogen atom is substituted by the bromine atom, as shown in Fig. 2. Vertical excitation energies and dominant excitations evaluated with OM2/CIS and LR-TDDFT/ωB97XD/cc-pVTZ (TD-ωB97XD) for m-rNDI are listed in Table 5. In the MNDO package, there do not exist parameters for the bromine atom. Therefore, we perform the excited-state calculation with parameters of the fluorine atom. For singlet excited states, OMx/CIS gives a very reasonable description of the excitation energies and dominant excitation configurations, while it slightly underestimates the excitation energies of $S_2$ ($n_{H-2} \rightarrow \pi_L$). A sequence of triplet excited states with dominant excitation of $\pi_H \rightarrow \pi_L$, $\pi_{H-1} \rightarrow \pi_L$ and $n_{H-2} \rightarrow \pi_L$ predicted by OM2/CIS is also consistent with those from TD-ωB97XD. The ultrafast intersystem crossing in rNDI takes place after an initial $\pi_{H-1} \rightarrow \pi_L$ excitation, namely $S_0 \rightarrow S_4$.

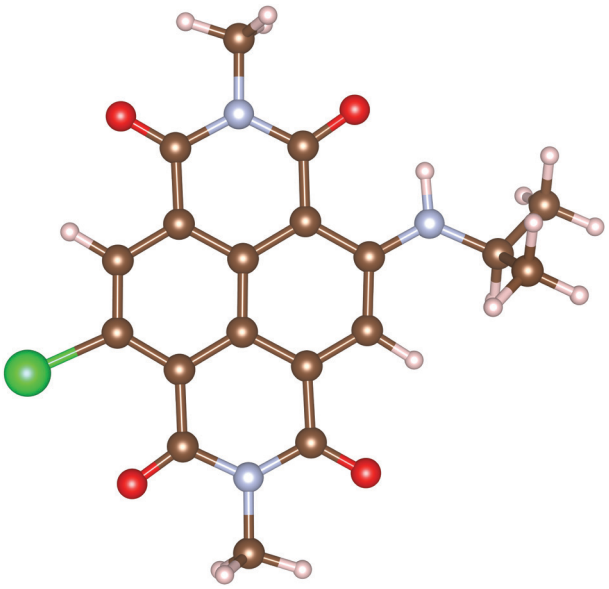

Fig. 2 Molecule structures of m-rNDI.

Table 5 Vertical excitation energies (in eV) and dominant excitations evaluated with OM2/CIS and LR-TDDFT/ωB97XD/cc-pVTZ for m-rNDI. The subscripts "H" and "L" indicate the HOMO and LUMO molecular orbitals. The subscripts "H−*i*" and "L−*i*" indicate the HOMO−*i* and LUMO−*i* molecular orbitals

| | OM2 | | ωB97XD | |
|---|---|---|---|---|
| | $\Delta E$ (eV) | Dominant excitation | $\Delta E$ (eV) | Dominant excitation |
| $S_1$ | 3.15 | $\pi_H \rightarrow \pi_L$ (0.94) | 3.05 | $\pi_H \rightarrow \pi_L$ (0.97) |
| $S_2$ | 3.72 | $n_{H-2} \rightarrow \pi_L$ (0.79) | 4.05 | $n_{H-2} \rightarrow \pi_L$ (0.79) |
| $S_3$ | 3.95 | $n_{H-7} \rightarrow \pi_L$ (0.54)<br>$n_{H-6} \rightarrow \pi_L$ (0.35) | 4.06 | $\pi_{H-1} \rightarrow \pi_L$ (0.91) |
| $S_4$ | 4.00 | $\pi_{H-1} \rightarrow \pi_L$ (0.76) | 4.44 | $\pi_H \rightarrow \pi_{L+1}$ (0.68)<br>$\pi_{H-3} \rightarrow \pi_L$ (0.63) |
| $T_1$ | 2.08 | $\pi_H \rightarrow \pi_L$ (0.90) | 1.83 | $\pi_H \rightarrow \pi_L$ (0.93) |
| $T_2$ | 2.77 | $\pi_{H-1} \rightarrow \pi_L$ (0.81) | 2.40 | $\pi_{H-1} \rightarrow \pi_L$ (0.86) |
| $T_3$ | 3.31 | $\pi_{H-5} \rightarrow \pi_L$ (0.51)<br>$\pi_H \rightarrow \pi_{L+1}$ (0.48) | 3.34 | $\pi_H \rightarrow \pi_{L+1}$ (0.65)<br>$\pi_{H-9} \rightarrow \pi_L$ (0.40) |
| $T_4$ | 3.5 | $n_{H-2} \rightarrow \pi_L$ (0.74) | 3.7 | $n_{H-2} \rightarrow \pi_L$ (0.73) |

Table 6 shows some typical SOCs for m-rNDI computed with OM2/CIS and TD-ωB97XD. Explicit OM2/CIS calculations with parameters of the fluorine atom result in relatively small SOCs since the bromine atom is much heavier than the fluorine atom. As a compromise scheme, we set the effective nuclear charge $Z_{eff}$ to be 1435, which is $Z_{eff}$ of the bromine atom obtained from eqn (27), and consequently the scale factor for the Gaussian basis functions to be 0.9, which roughly reproduces SOCs evaluated with TD-ωB97XD. As shown in Table 6, good agreement of SOCs between OM2/CIS and TD-ωB97XD is obtained. Here, typical strong SOCs are observed between $\pi_H \rightarrow \pi_L$ and $n_{H-2} \rightarrow \pi_L$. However, the SOC between $\pi_{H-1} \rightarrow \pi_L$ and $n_{H-2} \rightarrow \pi_L$, namely ($S_4/T_4$) at the OM2/CIS level ($S_3/T_4$ for TD-ωB97XD), is quite small compared to the former one. This implies that the direct intersystem crossing from the second bright excited state $S_4$ to the triplet state may be very slow due

Table 6 Typical SOCs (in $cm^{-1}$) for m-rNDI computed with OM2/CIS and TDDFT/ωB97XD/cc-pVTZ

| | $S_1/T_4$ | $S_2/T_1$ | $S_2/T_2$ | $S_2/T_3$ |
|---|---|---|---|---|
| OM2 | 94 | 96 | 20 | 136 |
| ωB97XD | 98 | 104 | 15 | 132 |

| | $S_4/T_1$ | $S_4/T_2$ | $S_4/T_3$ | $S_4/T_4$ |
|---|---|---|---|---|
| OM2 | 1 | 0 | 1 | 11 |
| ωB97XD | 5 | 1 | 2 ($S_4/T_4$) | 7 ($S_3/T_4$) |

to the small SOC. There are unavoided surface crossings between singlet and triplet states. For example, the energies of $S_3$ and $S_4$ are very close to each other, and the surface crossing is unavoided in rNDI. Similarly, unavoided surface crossings also happen between $S_2$ and $T_4/T_5$. In our numerical simulations, we identified the excited state according to the excitation configuration to avoid problems induced by unavoided surface crossings.

As a pilot application of the generalized surface hopping approach based on our semiempirical OM2/CIS method, we perform excited-state dynamics simulations after an initial $S_0 \rightarrow S_4$ excitation for m-rNDI to gain deep insight into ultrafast intersystem crossing dynamics. To account for the solvent effect, a Langevin thermostat was used to keep the temperature constant at 298 K with a friction coefficient $\gamma$ of 2.0 $ps^{-1}$.[41,96] The velocity-Verlet algorithm was used with a time step of 0.5 fs for the nuclear motion. 500 independent surface hopping trajectories of 2 ps were run.

Fig. 3 shows the time evolution of the populations of the lowest-lying singlet and triplet excited states averaged over all trajectories on the OM2/CIS potential surface. It is clear that the decay of the second bright state $S_4$ take place within a very short time scale (<100 fs). However, as the population of $S_4$ decreases, the population of $S_2$ increases very rapidly, while at the same time there is only little population of triplet states.

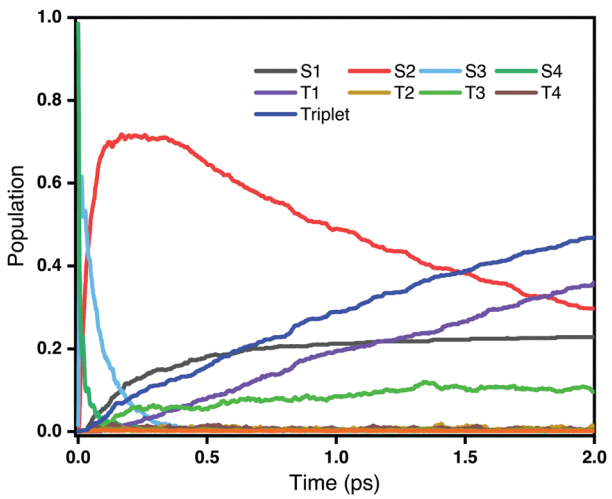


Fig. 3 Populations of different excited states as a function of time obtained from the fraction of trajectories in each state at the CIS/OM2 level. The initial excitation is $S_0 \rightarrow S_4$.

This reveals that the dominant decay channel of $S_4$ is through internal conversion to lower singlet states, namely $^1\pi\pi^* \rightarrow {}^1n\pi^*$. After 100 fs, with most $S_4$ decaying to $S_2$, there are two competing decay channels: one is a radiationless transition to $S_1$ through internal conversion, and the other is a transition to triplet states through intersystem crossing. As shown in Fig. 3, the populations of the $S_1$ and triplet states are almost equivalent at 1 ps. However, after that, the population of the triplet states, especially $T_1$, continuously increases. Overall, we conclude that ultrafast intersystem crossing after an initial excitation to the second bright state in rNDI mainly takes place between $^1n\pi^*$ and $^3\pi\pi^*$ instead of between $^1\pi\pi^*$ and $^3n\pi^*$.

## 5 Conclusion

We have presented efficient evaluation of SOC within the framework of OMx/CIS. The SOC Hamiltonian in terms of the one-electron Breit–Pauli operator and embodied effective nuclear charges is employed to evaluate SOCs between singlet states and a manifold of triplet states. Benchmark calculations on a set of small molecules show good agreement between the OMx/CIS method using the effective core potential basis set and the hybrid LR-TDDFT method using the all-electron basis set. However, analogous to the fact that the OMx/CIS method frequently underestimates molecular excitation energies,[41] the SOCs computed with OMx/CIS also show systematic deviations from those computed with LR-TDDFT. It is possible to optimize parameters, especially the scale factor $\zeta$ for integrals over Gaussian basis functions, to alleviate these deviations.

One particularly attractive application of the implementation of SOCs based on OMx/CIS is to extend the FSSH algorithm to simulate both internal conversion and intersystem crossing, namely radiationless transitions between electronic states with different spin multiplicity. Due to the high efficiency of the OMx/CIS method, all excited-state properties, including excitation energies, analytical energy gradients, nonadiabatic couplings and SOCs, can be computed "on the fly" with much less computational costs compared to *ab initio* methods. This semiempirical dynamics simulation method is able to provide a computationally accessible and reasonable description of photoinduced dynamics in large molecular systems consisting of hundreds of atoms on time scales of tens of picoseconds. As an initial application of this method, we perform a nonadiabatic dynamics simulation of c-NDIs after $S_0 \rightarrow S_4$ excitation and interpret the ultrafast intersystem crossing dynamics process which takes place on a very short time scale comparable to that for internal conversion processes.

## Conflicts of interest

There are no conflicts to declare.

## Acknowledgements

This work is supported by the National Natural Science Foundation of China (21688102, 22073086, 21803065, 21933011 and

 

21873112), by the National Key Research and Development Program of China (2016YFA0200604), and Anhui Initiative in Quantum Information Technologies (AHY090400).

## References

1 A. V. Akimov, A. J. Neukirch and O. V. Prezhdo, *Chem. Rev.*, 2013, **113**, 4496–4565.
2 S. Ardo and G. J. Meyer, *Chem. Soc. Rev.*, 2009, **38**, 115–164.
3 A. Hagfeldt, G. Boschloo, L. Sun, L. Kloo and H. Pettersson, *Chem. Rev.*, 2010, **110**, 6595–6663.
4 A. Kubacka, M. Fernández-García and G. Colón, *Chem. Rev.*, 2012, **112**, 1555–1614.
5 K. Maeda and K. Domen, *J. Phys. Chem. Lett.*, 2010, **1**, 2655–2661.
6 M. G. Walter, E. L. Warren, J. R. McKone, S. W. Boettcher, Q. Mi, E. A. Santori and N. S. Lewis, *Chem. Rev.*, 2010, **110**, 6446–6473.
7 T. Nelson, S. Fernandez-Alberti, A. E. Roitberg and S. Tretiak, *Acc. Chem. Res.*, 2014, **47**, 1155–1164.
8 F. Segatta, L. Cupellini, M. Garavelli and B. Mennucci, *Chem. Rev.*, 2019, **119**, 9361–9380.
9 J. C. Tully, *J. Chem. Phys.*, 2012, **137**, 22A301.
10 L. Wang, R. Long and O. V. Prezhdo, *Annu. Rev. Phys. Chem.*, 2015, **66**, 549–579.
11 R. Crespo-Otero and M. Barbatti, *Chem. Rev.*, 2018, **118**, 7026–7068.
12 B. F. Curchod and T. J. Martńez, *Chem. Rev.*, 2018, **118**, 3305–3336.
13 S. Mai, P. Marquetand and L. González, *Wiley Interdiscip. Rev.: Comput. Mol. Sci.*, 2018, **8**, e1370.
14 J. C. Tully, in *Modern Methods for Multidimensional Dynamics Computations in Chemistry*, ed. D. L. Thompson, World Scientific, Singapore, 1998, pp. 34–72.
15 M. Ben-Nun, J. Quenneville and T. J. Martńez, *J. Phys. Chem. A*, 2000, **104**, 5161–5175.
16 S. Pratihar, X. Ma, Z. Homayoon, G. L. Barnes and W. L. Hase, *J. Am. Chem. Soc.*, 2017, **139**, 3570–3590.
17 B. O. Roos, P. R. Taylor and P. E. M. Siegbahn, *Chem. Phys.*, 1980, **48**, 157–173.
18 K. Ruedenberg, M. W. Schmidt, M. M. Gilbert and S. T. Elbert, *Chem. Phys.*, 1982, **71**, 41–49.
19 K. Hirao, *Recent advances in multireference methods*, World Scientific, Singapore, 1999, vol. 4.
20 H. Lischka, M. Dallos, P. G. Szalay, D. R. Yarkony and R. Shepard, *J. Chem. Phys.*, 2004, **120**, 7322–7329.
21 K. Andersson and B. O. Roos, in *Modern electronic structure theory*, ed. D. R. Yarkony, World Scientific, Singapore, 1995, vol. 2 of Advanced Series in Physical Chemistry, pp. 55–109.
22 J. W. Snyder, B. F. E. Curchod and T. J. Martínez, *J. Phys. Chem. Lett.*, 2016, **7**, 2444–2449.
23 J. F. Stanton and R. J. Bartlett, *J. Chem. Phys.*, 1993, **98**, 7029–7039.
24 O. Christiansen, H. Koch and P. Jørgensen, *J. Chem. Phys.*, 1996, **105**, 1451–1459.
25 S. A. Kucharski, M. Wloch, M. Musial and R. J. Bartlett, *J. Chem. Phys.*, 2001, **115**, 8263–8266.
26 S. V. Levchenko and A. I. Krylov, *J. Chem. Phys.*, 2004, **120**, 175–185.
27 J. Schirmer, *Phys. Rev. A: At., Mol., Opt. Phys.*, 1982, **26**, 2395–2416.
28 A. Dreuw and M. Wormit, *Wiley Interdiscip. Rev.: Comput. Mol. Sci.*, 2015, **5**, 82–95.
29 M. E. Casida, in *Recent Advances in Density Functional Methods, Part I*, ed. D. P. Chong, World Scientific, River Edge, NJ, 1995, ch. 5, vol. I of Recent Advances in Computational Chemistry, pp. 155–192.
30 A. Dreuw and M. Head-Gordon, *Chem. Rev.*, 2005, **105**, 4009–4037.
31 C. Cisneros, T. Thompson, N. Baluyot, A. C. Smith and E. Tapavicza, *Phys. Chem. Chem. Phys.*, 2017, **19**, 5763–5777.
32 T. M. Cardozo, A. P. Galliez, I. Borges, F. Plasser, A. J. A. Aquino, M. Barbatti and H. Lischka, *Phys. Chem. Chem. Phys.*, 2019, **21**, 13916–13924.
33 G. Granucci, M. Persico and A. Toniolo, *J. Chem. Phys.*, 2001, **114**, 10608–10615.
34 A. Koslowski, M. E. Beck and W. Thiel, *J. Comput. Chem.*, 2003, **6**, 714–726.
35 W. Thiel, *Wiley Interdiscip. Rev.: Comput. Mol. Sci.*, 2014, **4**, 145–157.
36 D. Tuna, Y. Lu, A. Koslowski and W. Thiel, *J. Chem. Theory Comput.*, 2016, **12**, 4400–4422.
37 R. Mitrić, U. Werner, M. Wohlgemuth, G. Seifert and V. Bonačić-Koutecký, *J. Phys. Chem. A*, 2009, **113**, 12700–12705.
38 S. Tretiak and S. Mukamel, *Chem. Rev.*, 2002, **102**, 3171–3212.
39 P. O. Dral, X. Wu, L. Spörkel, A. Koslowski and W. Thiel, *J. Chem. Theory Comput.*, 2016, **12**, 1097–1120.
40 P. O. Dral, X. Wu, L. Spörkel, A. Koslowski, W. Weber, R. Steiger, M. Scholten and W. Thiel, *J. Chem. Theory Comput.*, 2016, **12**, 1082–1096.
41 J. Liu and W. Thiel, *J. Chem. Phys.*, 2018, **148**, 154103.
42 J. Liu and W. Thiel, *J. Chem. Phys.*, 2018, **148**, 244108.
43 E. van Lenthe, E. J. Baerends and J. G. Snijders, *J. Chem. Phys.*, 1993, **99**, 4597.
44 E. van Lenthe, E. J. Baerends and J. G. Snijders, *J. Chem. Phys.*, 1994, **10**, 9783.
45 E. van Lenthe, J. G. Snijders and E. J. Baerends, *J. Chem. Phys.*, 1996, **105**, 6505.
46 S. Koseki, M. S. Gordon, M. W. Schmidt and N. Matsunaga, *J. Phys. Chem.*, 1995, **99**, 12764–12772.
47 S. Koseki, M. W. Schmidt and M. S. Gordon, *J. Phys. Chem. A*, 1998, **102**, 10430–10435.
48 D. G. Fedorov, S. Koseki, M. W. Schmidt and M. S. Gordon, *Int. Rev. Phys. Chem.*, 2003, **22**, 551–592.
49 S. G. Chiodo and N. Russo, *J. Comput. Chem.*, 2009, **30**, 832–839.
50 M. Barbatti, M. Ruckenbauer, F. Plasser, J. Pittner, G. Granucci, M. Persico and H. Lischka, *Wiley Interdiscip. Rev.: Comput. Mol. Sci.*, 2014, **4**, 26–33.

51 F. Neese, F. Wennmohs, U. Becker and C. Riplinger, *J. Chem. Phys.*, 2020, **152**, 224108.
52 Y. Shao, Z. Gan, E. Epifanovsky, A. T. B. Gilbert, M. Wormit, J. Kussmann, A. W. Lange, A. Behn, J. Deng, X. Feng, D. Ghosh, M. Goldey, P. R. Horn, L. D. Jacobson, I. Kaliman, R. Z. Khaliullin, T. Kús, A. Landau, J. Liu, E. I. Proynov, Y. M. Rhee, R. M. Richard, M. A. Rohrdanz, R. P. Steele, E. J. Sundstrom, H. L. Woodcock III, P. M. Zimmerman, D. Zuev, B. Albrecht, E. Alguire, B. Austin, G. J. O. Beran, Y. A. Bernard, E. Berquist, K. Brandhorst, K. B. Bravaya, S. T. Brown, D. Casanova, C.-M. Chang, Y. Chen, S. H. Chien, K. D. Closser, D. L. Crittenden, M. Diedenhofen, R. A. DiStasio Jr., H. Dop, A. D. Dutoi, R. G. Edgar, S. Fatehi, L. Fusti-Molnar, A. Ghysels, A. Golubeva-Zadorozhnaya, J. Gomes, M. W. D. Hanson-Heine, P. H. P. Harbach, A. W. Hauser, E. G. Hohenstein, Z. C. Holden, T.-C. Jagau, H. Ji, B. Kaduk, K. Khistyaev, J. Kim, J. Kim, R. A. King, P. Klunzinger, D. Kosenkov, T. Kowalczyk, C. M. Krauter, K. U. Lao, A. Laurent, K. V. Lawler, S. V. Levchenko, C. Y. Lin, F. Liu, E. Livshits, R. C. Lochan, A. Luenser, P. Manohar, S. F. Manzer, S.-P. Mao, N. Mardirossian, A. V. Marenich, S. A. Maurer, N. J. Mayhall, C. M. Oana, R. Olivares-Amaya, D. P. O'Neill, J. A. Parkhill, T. M. Perrine, R. Peverati, P. A. Pieniazek, A. Prociuk, D. R. Rehn, E. Rosta, N. J. Russ, N. Sergueev, S. M. Sharada, S. Sharmaa, D. W. Small, A. Sodt, T. Stein, D. Stück, Y.-C. Su, A. J. W. Thom, T. Tsuchimochi, L. Vogt, O. Vydrov, T. Wang, M. A. Watson, J. Wenzel, A. White, C. F. Williams, V. Vanovschi, S. Yeganeh, S. R. Yost, Z.-Q. You, I. Y. Zhang, X. Zhang, Y. Zhou, B. R. Brooks, G. K. L. Chan, D. M. Chipman, C. J. Cramer, W. A. Goddard III, M. S. Gordon, W. J. Hehre, A. Klamt, H. F. Schaefer III, M. W. Schmidt, C. D. Sherrill, D. G. Truhlar, A. Warshel, X. Xua, A. Aspuru-Guzik, R. Baer, A. T. Bell, N. A. Besley, J.-D. Chai, A. Dreuw, B. D. Dunietz, T. R. Furlani, S. R. Gwaltney, C.-P. Hsu, Y. Jung, J. Kong, D. S. Lambrecht, W. Liang, C. Ochsenfeld, V. A. Rassolov, L. V. Slipchenko, J. E. Subotnik, T. Van Voorhis, J. M. Herbert, A. I. Krylov, P. M. W. Gill and M. Head-Gordon, *Mol. Phys.*, 2015, **113**, 184–215.
53 G. M. J. Barca, C. Bertoni, L. Carrington, D. Datta, N. De Silva, J. E. Deustua, D. G. Fedorov, J. R. Gour, A. O. Gunina, E. Guidez, T. Harville, S. Irle, J. Ivanic, K. Kowalski, S. S. Leang, H. Li, W. Li, J. J. Lutz, I. Magoulas, J. Mato, V. Mironov, H. Nakata, B. Q. Pham, P. Piecuch, D. Poole, S. R. Pruitt, A. P. Rendell, L. B. Roskop, K. Ruedenberg, T. Sattasathuchana, M. W. Schmidt, J. Shen, L. Slipchenko, M. Sosonkina, V. Sundriyal, A. Tiwari, J. L. Galvez Vallejo, B. Westheimer, M. Wloch, P. Xu, F. Zahariev and M. S. Gordon, *J. Chem. Phys.*, 2020, **152**, 154102.
54 *TURBOMOLE V. 6.3.1, a development of University of Karlsruhe and Forschungszentrum Karlsruhe GmbH, 1989-2007, TURBOMOLE GmbH, since 2007*, available from http://www.turbomole.com.
55 M. Barbatti, *Wiley Interdiscip. Rev.: Comput. Mol. Sci.*, 2011, **1**, 620–633.
56 E. Fabiano, T. W. Keal and W. Thiel, *Chem. Phys.*, 2008, **349**, 334–347.
57 L. Spörkel and W. Thiel, *J. Chem. Phys.*, 2016, **144**, 194108.
58 V. Wintgens, P. Valat, J. Kossanyi, L. Biczok, A. Demeter and T. Berces, *J. Chem. Soc., Faraday Trans.*, 1994, **90**, 411.
59 T. C. Barros, S. Brochsztain, V. G. Toscano, P. Berci Filho and M. J. Politi, *J. Photochem. Photobiol., A*, 1997, **111**, 97.
60 S. Alp, S. Erten, C. Karapire, B. Koz, A. O. Doroshenko and S. Icli, *J. Photochem. Photobiol., A*, 2000, **135**, 103.
61 M. S. Refat, I. Grabchev, J. M. Chovelon and G. Ivanova, *Spectrochim. Acta, Part A*, 2006, **64**, 435.
62 O. Yushchenko, G. Licari, S. Mosquera-Vazquez, N. Sakai, S. Matile and E. Vauthey, *J. Phys. Chem. Lett.*, 2015, **6**, 2096–2100.
63 E. R. Davidson, *J. Comput. Phys.*, 1975, **17**, 87–94.
64 C. Zener, *Proc. R. Soc. London, Ser. A*, 1932, **137**(833), 696–702.
65 C. Xu, L. Yu, C. Zhu, J. Yu and Z. Cao, *Sci. Rep.*, 2016, **6**, 26768.
66 B. Maiti and G. C. Schatz, *J. Chem. Phys.*, 2003, **119**, 12360–12371.
67 G. Granucci, M. Persico and G. Spighi, *J. Chem. Phys.*, 2012, **137**, 22A501.
68 G. Cui and W. Thiel, *J. Chem. Phys.*, 2014, **14**, 124101.
69 S. Mai, P. Marquetand and L. González, *Int. J. Quantum Chem.*, 2015, **115**, 1215–1231.
70 B. F. E. Curchod, C. Rauer, P. Marquetand, L. González and T. J. Martínez, *J. Chem. Phys.*, 2016, **144**, 101102.
71 J. Peng, Y. Xie, D. Hu and Z. Lan, *J. Chem. Phys.*, 2019, **150**, 164126.
72 B. Fu, B. C. Shepler and J. M. Bowman, *J. Am. Chem. Soc.*, 2011, **133**, 7957–7968.
73 B. F. Habenicht and O. V. Prezhdo, *J. Am. Chem. Soc.*, 2012, **134**, 15648–15651.
74 F. Franco de Carvalho and I. Tavernelli, *J. Chem. Phys.*, 2015, **143**, 224105.
75 M. Richter, P. Marquetand, J. González-Vázquez, I. Sola and L. González, *J. Phys. Chem. Lett.*, 2012, **3**, 3090–3095.
76 L. Martínez-Fernández, I. Corral, G. Granucci and M. Persico, *Chem. Sci.*, 2014, **5**, 1336–1347.
77 A. J. Atkins and L. González, *J. Phys. Chem. Lett.*, 2017, **8**, 3840–3845.
78 W. Thiel, *MNDO99 program*, Max-Planck-Institut für Kohlenforschung, Mülheim, Germany, 2007. Available from the author upon private communication.
79 S. Koseki, N. Matsunaga, T. Asada, M. W. Schmidt and M. S. Gordon, *J. Phys. Chem. A*, 2019, **123**, 2325–2339.
80 W. J. Stevens, H. Basch and M. Krauss, *J. Chem. Phys.*, 1984, **81**, 6026–6033.
81 S. G. Chiodo and M. Leopoldini, *Comput. Phys. Commun.*, 2014, **185**, 676–683.
82 X. Gao, S. Bai, D. Fazzi, T. Niehaus, M. Barbatti and W. Thiel, *J. Chem. Theory Comput.*, 2017, **13**, 515–524.
83 K. Momma and F. Izumi, *J. Appl. Crystallogr.*, 2008, **41**, 653–658.
84 A. D. Becke, *J. Chem. Phys.*, 1993, **98**, 1372–1377.

 

85 J.-D. Chai and M. Head-Gordon, *Phys. Chem. Chem. Phys.*, 2008, **10**, 6615–6620.
86 S. G. Chiodo and N. Russo, *Chem. Phys. Lett.*, 2010, **490**, 90–96.
87 J. Pirillo, B. De Simone and N. Russo, *Theor. Chem. Acc.*, 2016, **135**, 8.
88 S. Bhosale, A. L. Sisson, P. Talukdar, A. Fürstenberg, N. Banerji, E. Vauthey, G. Bollot, J. Mareda, C. Röger and F. Würthner, *Science*, 2006, **313**, 84.
89 A. L. Sisson, N. Sakai, N. Banerji, A. Fürstenberg, E. Vauthey and S. Matile, *Angew. Chem., Int. Ed.*, 2008, **47**, 3727.
90 N. Sakai, M. Lista, O. Kel, S.-i. Sakurai, D. Emery, J. Mareda, E. Vauthey and S. Matile, *J. Am. Chem. Soc.*, 2011, **133**, 15224.
91 N. Sakai, J. Mareda, E. Vauthey and S. Matile, *Chem. Commun.*, 2010, **46**, 4225.
92 D. Villamaina, M. M. A. Kelson, S. V. Bhosale and E. Vauthey, *Phys. Chem. Chem. Phys.*, 2014, **16**, 5188.
93 S. V. Bhosale, S. V. Bhosale, M. B. Kalyankar and S. J. Langford, *Org. Lett.*, 2009, **11**, 5418.
94 C. Röger and F. Würthner, *J. Org. Chem.*, 2007, **72** 8070.
95 F. Würthner, A. Shahadat, C. Thalacker and T. Debaerdemaeker, *Chem. – Eur. J.*, 2002, **8**, 4742.
96 M. G. Paterlini and D. M. Ferguson, *Chem. Phys.*, 1998, **236**, 243–252.